REPORT

www.the-innovation.org

3D-bioprinted anisotropic bicellular living hydrogels boost osteochondral regeneration via reconstruction of cartilage–bone interface

Yijian Zhang,[1,5] Duo Li,[2,3,5] Yang Liu,[1,5] Liuqi Peng,[2] Dongdong Lu,[1] Pinpin Wang,[2] Dongxu Ke,[4] Huilin Yang,[1,*] Xuesong Zhu,[1,*] and Changshun Ruan[2,3,*]
*Correspondence: suzhouspine@163.com (H.Y.); zhuxs@suda.edu.cn (X.Z.); cs.ruan@siat.ac.cn (C.R.)
Received: July 27, 2023; Accepted: November 17, 2023; Published Online: November 20, 2023; https://doi.org/10.1016/j.xinn.2023.100542

GRAPHICAL ABSTRACT

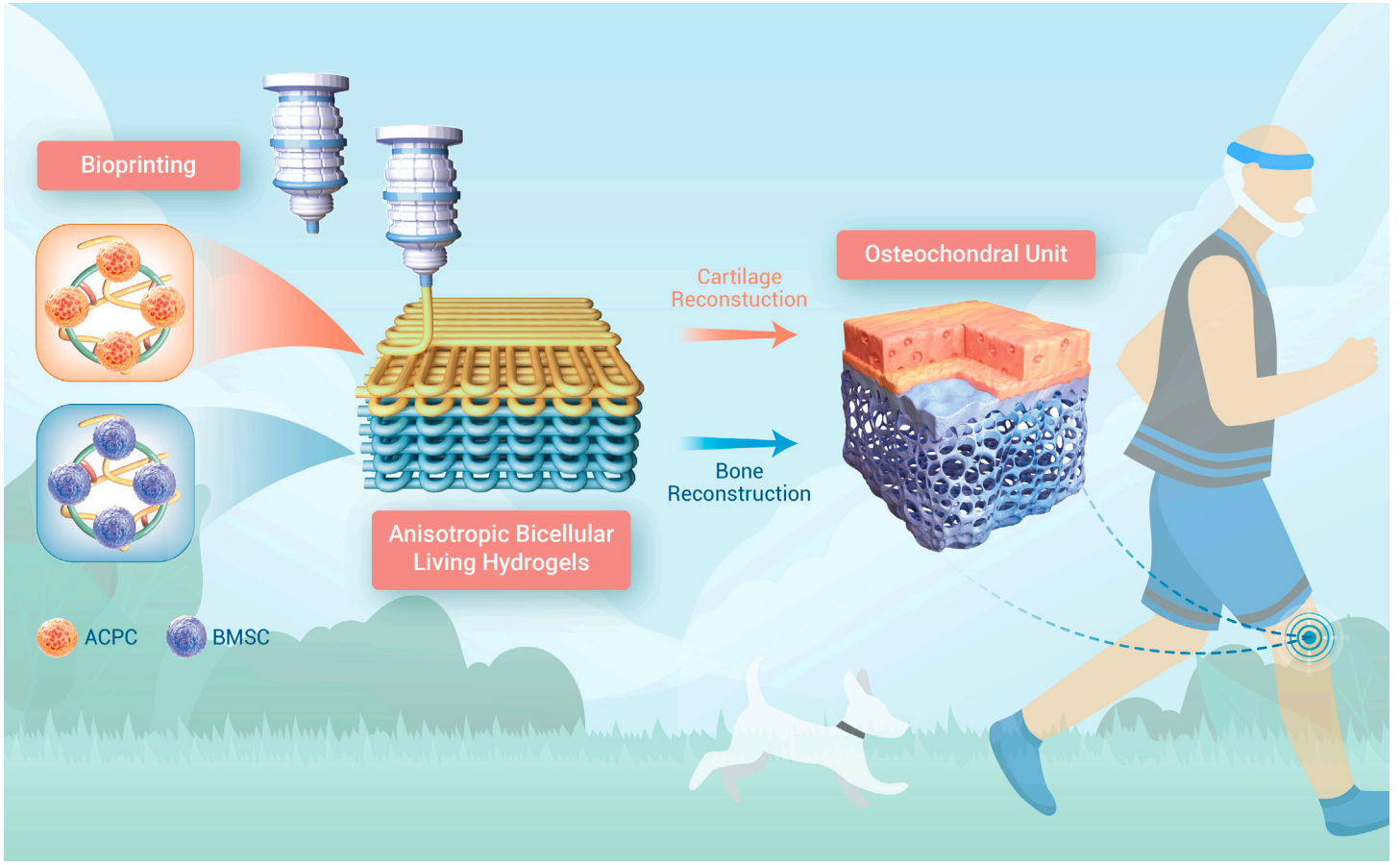

PUBLIC SUMMARY

- Anisotropic bicellular living hydrogels (ABLHs) were bioprinted at room temperature with high cell viability.
- ABLHs promoted osteochondral regeneration by fulfilling osteogenesis and chondrogenesis.
- Cartilage-bone-vessel crosstalk was confirmed to lead to the reconstruction of the osteochondral interface.

REPORT

3D-bioprinted anisotropic bicellular living hydrogels boost osteochondral regeneration via reconstruction of cartilage–bone interface

Yijian Zhang,[1,5] Duo Li,[2,3,5] Yang Liu,[1,5] Liuqi Peng,[2] Dongdong Lu,[1] Pinpin Wang,[2] Dongxu Ke,[4] Huilin Yang,[1,*] Xuesong Zhu,[1,*] and Changshun Ruan[2,3,*]

[1]Department of Orthopaedics, The First Affiliated Hospital of Soochow University, Soochow University, Suzhou 215006, China

[2]Research Center for Human Tissue and Organ Degeneration, Institute of Biomedicine and Biotechnology, Shenzhen Institute of Advanced Technology, Chinese Academy of Sciences, Shenzhen 518055, China

[3]University of Chinese Academy of Sciences, Beijing 100049, China

[4]Novaprint Therapeutics Suzhou Co., Ltd., Room 605, B1 Building, BioBay, No.218 Xinghu Street, Suzhou Industrial Park, Suzhou 215000, China

[5]These authors contributed equally

*Correspondence: suzhouspine@163.com (H.Y.); zhuxs@suda.edu.cn (X.Z.); cs.ruan@siat.ac.cn (C.R.)

Received: July 27, 2023; Accepted: November 17, 2023; Published Online: November 20, 2023; https://doi.org/10.1016/j.xinn.2023.100542

Citation: Zhang Y., Li D., Liu Y., et al., (2024). 3D-bioprinted anisotropic bicellular living hydrogels boost osteochondral regeneration via reconstruction of cartilage–bone interface. The Innovation **5(1)**, 100542.

Reconstruction of osteochondral (OC) defects represents an immense challenge due to the need for synchronous regeneration of special stratified tissues. The revolutionary innovation of bioprinting provides a robust method for precise fabrication of tissue-engineered OCs with hierarchical structure; however, their spatial living cues for simultaneous fulfilment of osteogenesis and chondrogenesis to reconstruct the cartilage-bone interface of OC are underappreciated. Here, inspired by natural OC bilayer features, anisotropic bicellular living hydrogels (ABLHs) simultaneously embedding articular cartilage progenitor cells (ACPCs) and bone mesenchymal stem cells (BMSCs) in stratified layers were precisely fabricated via two-channel extrusion bioprinting. The optimum formulation of the 7% GelMA/3% AlgMA hydrogel bioink was demonstrated, with excellent printability at room temperature and maintained high cell viability. Moreover, the chondrogenic ability of ACPCs and the osteogenic ability of BMSCs were demonstrated *in vitro*, confirming the inherent differential spatial regulation of ABLHs. In addition, ABLHs exhibited satisfactory synchronous regeneration of cartilage and subchondral bone *in vivo*. Compared with homogeneous hydrogels, the neo-cartilage and neo-bone in ABLHs were augmented by 23.5% and 20.8%, respectively, and more important, a more harmonious cartilage–bone interface was achieved by ABLHs due to their well-tuned cartilage-bone-vessel crosstalk. We anticipate that such a strategy of tissue-mimetic ABLH by means of bioprinting is capable of spatiotemporal cell-driven regeneration, offering insights into the fabrication of anisotropic living materials for the reconstruction of complex organ defects.

INTRODUCTION

Osteochondral (OC) defects are becoming a serious global health problem as increases in the aging population and rates of athletic injury occur, imposing substantial social and economic burdens.[1] Owing to their intrinsically poor regenerative capacity, current therapeutic interventions are far from satisfactory.[2] Tissue-engineered implants provide mechanical support for the defect region and serve as bioactive factor carriers to recruit *in situ* cells or reshape the local adverse microenvironment, suggesting a potential alternative approach for OC regeneration.[3-5] Recently, the introduction of exogenous pluripotent stem cells with the potential to broadly differentiate into inanimate biomaterials further improved the repair capacity for tissue damage[6]; however, limited cell survival and chaotic cell distribution in traditional implants remain grand challenges. Moreover, unlike uniform tissues (eg, individual cartilage, bone), the specific stratified structure of the OC unit comprises superficial chondroid extracellular matrix (C-ECM) and deep osteoid ECM (O-ECM); thus, the reconstruction of OC must take both phases into consideration. Accordingly, a scheme capable of receiving "living cues" with abundant embedded cells and the capacity for "spatial regulation" with simultaneous tissue-specific allocation seems to be a revitalized approach for OC repair.

Three-dimensional (3D) bioprinting technology that can directly customize cell-laden constructs via the use of a mixture of cells and biomaterials as bioinks provides new possibilities for OC tissue engineering.[7] Bioprinted stratified electrowritten fiber-reinforced hydrogel with a trilayered structure mimics native OC and thus is a candidate for use in the regeneration of OC defects.[8] In our previous study, we designed a 3D-bioprinted multilayer scaffold laden with bone marrow–derived mesenchymal stem cells (BMSCs) for repairing OC defects; however, the lack of exogenous cells in the bottom bone layer impeded the reshaping of the integrated OC interface.[9] In addition, the bioprinting-assisted development of biomaterials for OC repair still faces two critical issues. One technical challenge is the maintenance of cell viability during the complex fabrication process of OC-inspired stratified structures.[10] One of the most traditional bioinks, methacryloyl gelatin (GelMA), has improved accessibility to bioprinting due to its excellent printing capabilities and quick light crosslinking. However, it displays obvious limitations in an operating environment that is unsuitable for cell survival.[11] Considering the prolonged cultivation period of bioink, an inhospitable microenvironment not only impedes cellular viability but also compromises the potential for cellular differentiation and restructuring of the ECM. The other puzzle seems to be the spatial variations in chondrocytes and osteoblasts in a hierarchical OC unit, which requires precise tissue-specific cell supplementation. Of note, osteogenic and chondrogenic lineage commitment are mechanistically distinct processes. To achieve the directed differentiation of stem cells, in most existing measures, the incorporation of growth factors (transforming growth factor- β1 [TGF-β1] or bone morphogenetic protein 2 [BMP2])[12] or small-molecule compounds (melatonin or kartogenin)[13] into the stratified layers of OC implants was adopted. Nevertheless, exploiting the process of bioprinting, the precise load of the inherent spatial distribution of different cells to directly generate an anisotropic living construct has been less emphasized for OC regeneration.

To address these challenges, inspired by the natural bilayer structure of the OC unit consisting of upper C-ECM plus chondrocytes and lower O-ECM plus BMSCs, anisotropic bicellular living hydrogels (ABLHs) were innovatively fabricated via a two-channel extrusion-based bioprinting technique in this study. Composite hydrogels made from GelMA and methacryloyl alginate (AlgMA) were investigated as customized bioinks for the biofabrication of ABLHs at room temperature and subsequently provided a suitable nest site for cell survival and growth. Cartilage-derived articular cartilage progenitor cells (ACPCs) and bone-derived BMSCs were allocated to the stratified layers of ABLHs to ensure the respective cartilage- or bone-oriented lineage commitment. Furthermore, the *in vivo* synchronous regenerative ability of ABLHs for cartilage and subchondral bone was evaluated by implantation in a rabbit model of OC defects. In addition, with the aid of temporal transcriptome analysis, the mechanisms of ABLH-induced proregenerative effects were comprehensively revealed, in which the crosstalk between osteogenesis, chondrogenesis, and angiogenesis was orchestrated in the regeneration of anisotropic OC units.

RESULTS AND DISCUSSION

Fabrication of ABLHs via a customized bioink of photocurable GelMA/AlgMA

Based on the exceptional biocompatibility of GelMA and easy operability of AlgMA, the composite hydrogels of GelMA and AlgMA were investigated as customized bioinks for the fabrication of ABLHs. As a bioink for extrusion-based bioprinting, an ideal shear-thinning behavior is crucial to the high fidelity of the printed structure. When GelMA and AlgMA were mixed, compounded bioinks maintained effective shear-thinning behaviors (Figure 1A) and temperature-relevant moduli (Figure 1B). Methacryloyl groups convey efficacious

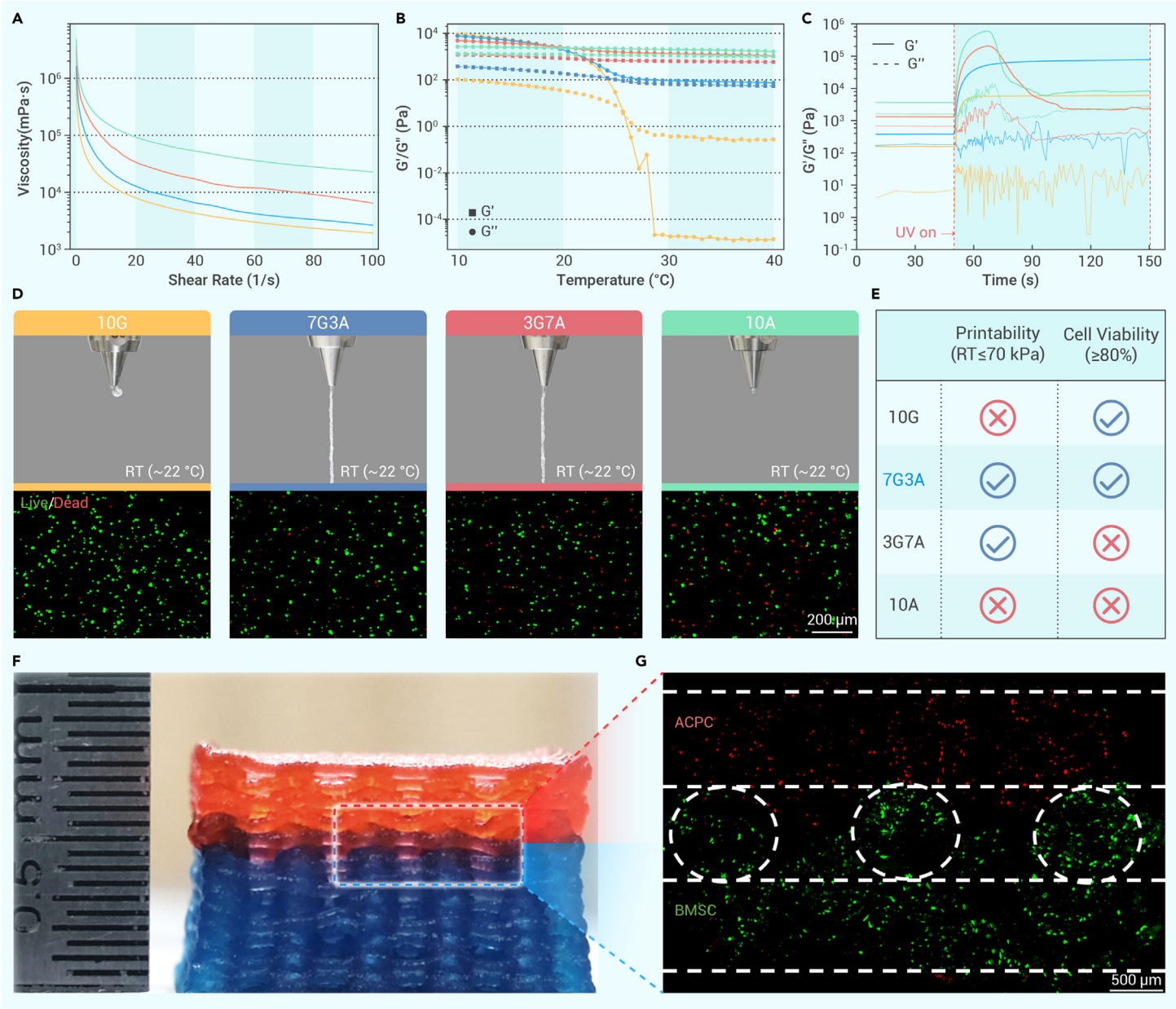

Figure 1. Preparation and printability of 7G3A compounded bioinks (A–G) Rheological measurements provided evidence for the shear thinning (A), temperature-programmable viscosity (B), and photocrosslinking process (C) of the GelMA and AlgMA compounded bioinks. Extrusion behavior (D) of bioinks at room temperature (~22°C) with proper pressure and cell viability (E) inside after crosslinking. Cell density 2×10^7/mL. Scale bar, 100 μm. 7G3A was chosen as the best bioink radio (F) and the cell-laden structure established by it (G). In the bilayer structure, the upper layer encapsulated ACPCs, which is red in the fluorescence image, and the green represents BMSCs in the lower layer. Scale bar, 500 μm.

photocrosslinking points, revealing a quick crosslinking process (approximately 5 s) to each single or compounded bioink (Figure 1C). These rheological results provided profitable advantages for compounded bioinks, enabling them to be directly printed at room temperature with cell-friendly extrusion pressure (≤ 70 kPa) (Figure 1D) and maintaining constructs in a stable structure after photocrosslinking.[14] Moreover, cells encapsulated in different crosslinked bioinks displayed different cell viabilities. With an increase in AlgMA content, the cell death rate increased. The group 7G3A bioink possessed 85.7% living cells, which is extremely close to that of the group 10G bioink (87.6%) (Figures 1E and S1A). Taking printability and cell viability into consideration, 7G3A was the best ratio to be explored for further investigation (Figure 1F). In addition, after photocrosslinking, 7G3A hydrogels demonstrated a water swelling ratio of 916.10% ± 4.97% (Figure S1B) and a degradation period of more than 5 weeks (Figure S1C). Compression tests showed that the 7G3A hydrogels had stronger mechanical properties than GelMA alone (Figures S1D–S1F) and were adaptable for OC regeneration. Based on 7G3A bioinks, several structures with cells inside were successfully fabricated, such as a high-fidelity and integrated ABLHs (12 mm width and 8 mm height) with ACPCs above (3 mm height) and BMSCs below (5 mm height) (Figures 1F and 1G). Letters (Figure S2A) and cylinders (Figure S2B) were constructed as well. The cells inside were homogeneously distributed (Figure S2C) and had interactions with the matrix, indicating that 7G3A did not limit cell adhesion and growth (Figure S2D).

Heterogeneous lineage differentiation of ABLHs *in vitro*

To enable dichotomous chondrogenic and osteogenic differentiation elicited from the natural stratified cellular composition in the OC unit, chondroprogenitor ACPCs and osteoprogenitor BMSCs isolated from rabbit cartilage and bone marrow, respectively, were characterized and compared in monolayer culture *in vitro*. The cultured ACPCs or BMSCs highly expressed CD29 and CD90 markers but were negative for CD34 and CD45, confirming the stemness of these two cell types (Figure S3). The trilineage differentiation further revealed that BMSCs possessed superior adipogenic and osteogenic differentiation abilities, whereas ACPCs showed greater chondrogenic properties (Figure S4). The cell morphology was comparable between the two cell types; however, the clonogenic and proliferative capacities were stronger in BMSCs than in ACPCs (Figures 2A–2C). Here, bone-initiated BMSCs and cartilage-initiated ACPCs

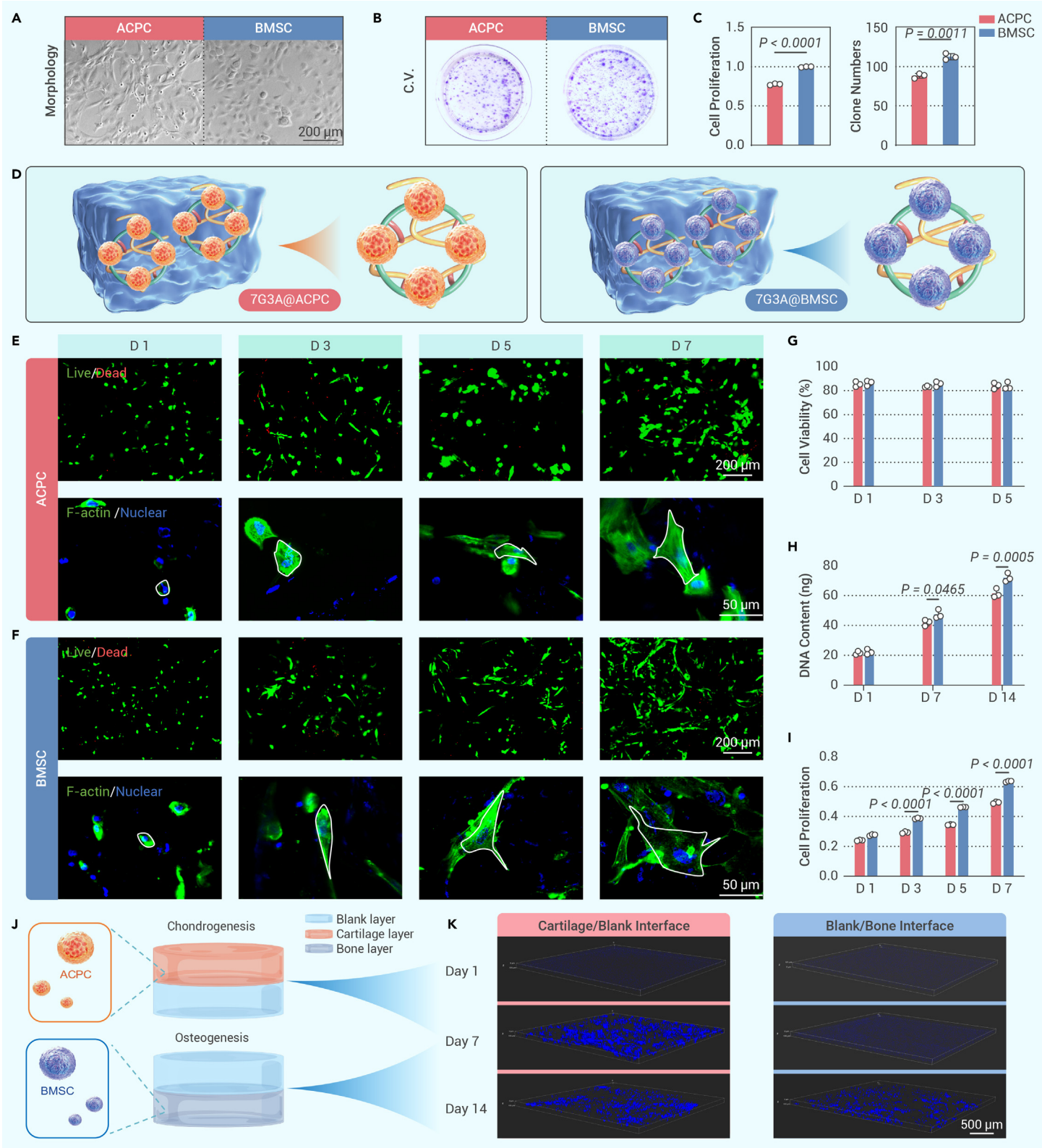

Figure 2. The 7G3A composite bioprinted hydrogels supported the survival and proliferation of embedded cells (A and B) The morphology and crystal violet staining of ACPCs and BMSCs. (C) Quantitative analysis of the cell proliferation rate and clone number between ACPCs and BMSCs in *in vitro* 2D culture (n = 4). (D) Schematic illustration of 3D bioprinted constructs laden with ACPCs or BMSCs. (E and F) Cell viability was determined by dead/live staining, and cell spreading was assessed by cytoskeleton staining (white dashed lines indicate the cell boundary). (G–I) Quantification of cell viability (G), DNA content (H), and cell proliferation assays (I) (n = 4). (J) ACPCs encapsulated in 7G3A formed a cartilage layer, BMSCs encapsulated in 7G3A formed a bone layer, and the blank layer indicated that no cells were contained. (K) Different layers of the compounded scaffold were cultured in cartilage or bone-differentiated culture medium for 2 weeks The 3D figures were captured by confocal microscopy, and cells were labeled with DAPI dye. Data are shown as the mean ± SD. Statistical significance was determined by unpaired Student's t-test.

were chosen as catalysts for optimal adaptation in constructing an OC-mimic unit that facilitates the regeneration of both bone and cartilage matrices. Subsequently, ACPC- or BMSC-laden hydrogels were prepared using 3D bioprinting (Figures 2D and 2E). Owing to the advantages of printability at physiological temperature, bioprinted hydrogels encouraged the survival, proliferation, and spreading of internal cells in an environmentally suitable niche

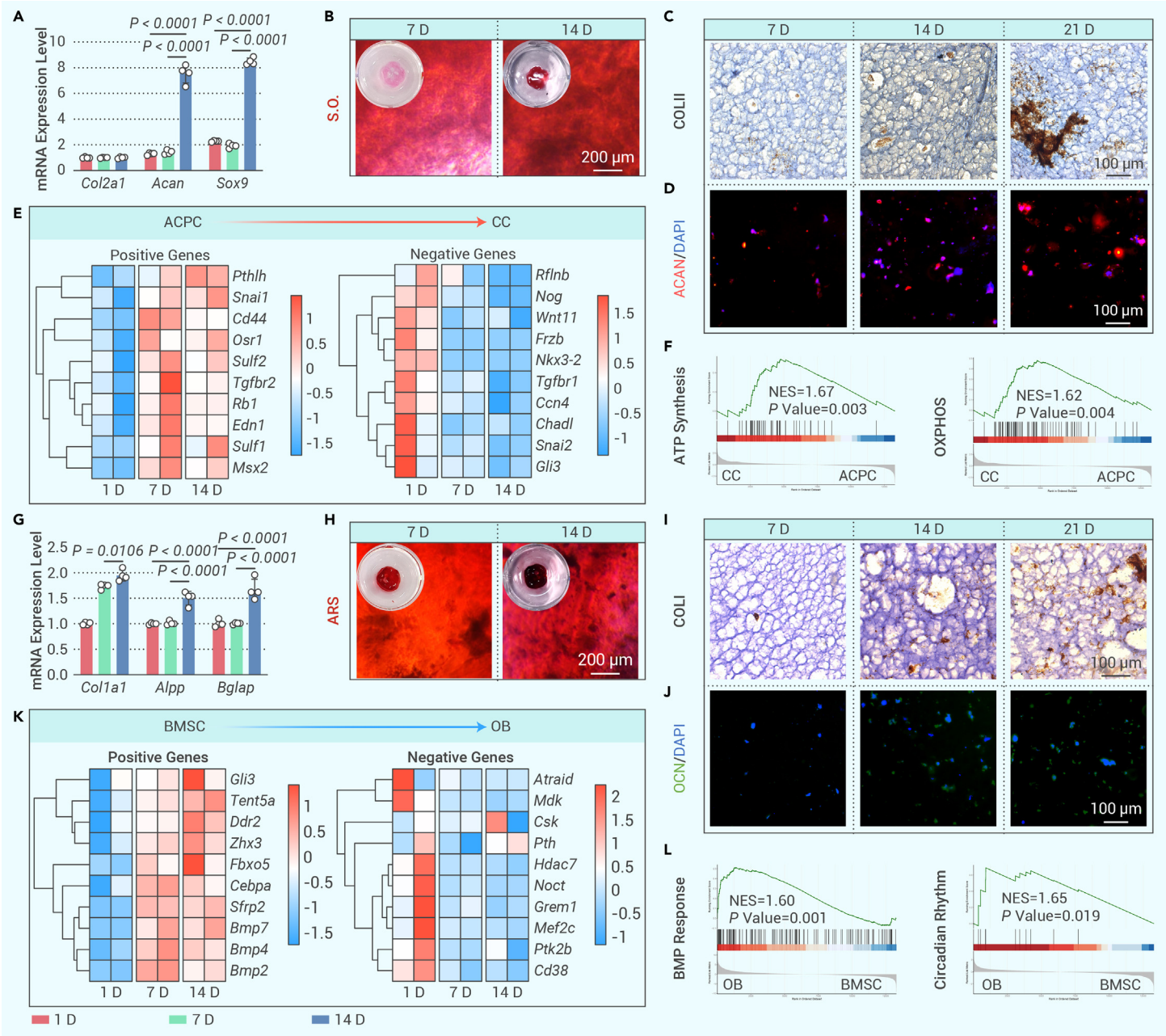

Figure 3. Distinct lineage commitment toward chondrogenesis or osteogenesis in ACPC- or BMSC-laden bioprinted constructs (A) Chondrogenic gene expression levels were measured by quantitative real-time PCR (n = 4). (B) C-ECM was visualized by Safranin O staining. (C and D) Immunohistochemical staining for the C-ECM markers COLII and ACAN. (E) Heatmaps of DEGs associated with chondrogenic differentiation. (F) GSEA of key events involved in chondrogenic differentiation. (G) Osteogenic gene expression levels were measured by quantitative real-time PCR (n = 4). (H) O-ECM was visualized by alizarin red staining. (I and J) Immunohistochemical staining for the O-ECM markers COLI and OCN. (K) Heatmaps of DEGs associated with osteogenic differentiation. (L) GSEA of key events involved in osteogenic differentiation. Data are shown as the mean ± SD. Statistical significance was determined by ANOVA.

(Figures 2E–2G). Consistent with 2D culture, the 3D-cultured BMSCs were more proliferative than the ACPCs in hydrogels (Figures 2H and 2I). Cell behaviors were preliminarily observed in an *in vitro* bilayer model with one acellular layer and the other encapsulating cells (Figure 2J). ACPCs and BMSCs spread out within 7 or 14 days, respectively, under the influence of their specialized lineage differentiations (Figure 2K). In the initial stages, the designed interface exhibited stability and clarity, whereas the ambiguous interface was maintained after 1 week of culture *in vitro* along with cell proliferation, migration, and differentiation.

To further evaluate the directional differentiation potential of the two cell types at early or late stages, ACPC- or BMSC-laden hydrogels were exposed to chondrogenic or osteogenic culture media for 7 or 14 days of induction, respectively. Expression levels of cartilage-specific genes (*Col2a1*, *Acan*, and *Sox9*) progressively increased during *in vitro* differentiation (Figure 3A). Safranin O staining exhibited a gradual improvement in C-ECM in ACPC-laden hydrogels (Figures 3B and S5). Further immunohistological (IHC) assays confirmed that expression of collagen type II (COLII) and aggrecan (ACAN), the main components of C-ECM, was significantly increased in the 3D-culture platform (Figures 3C, 3D, and S6). According to the pseudotime-based differentially expressed gene (DEG) heatmap, positive-regulated genes of chondrogenesis, expression levels of parathyroid hormone-like hormone (*Pthlh*),[15] odd-skipped related transcription factor 1 (*Osr1*),[16] and sulfatase (*Sulf)1/2*[17], were increased, but expression levels of negative-regulated genes noggin (*Nog*),[18] cellular communication network factor 4 (*Ccn4*),[19] and chondroadherin-like (*Chadl*),[20] were suppressed (Figure 3E). The in-depth pathway analysis indicated that activated mitochondrial ATP synthesis and oxidative phosphorylation were implicated in ACPC differentiation toward the chondrocyte lineage (Figures 3F, S6, and S7). Indeed, mitochondria-mediated energy metabolism, redox balance, and cellular respiration are of paramount importance to the stem cell differentiation program.[21] Our recent study elucidated that the impairment of mitochondrial respiratory chain complex functions aggravates the progression of osteoarthritis.[22] Based on the plant-derived

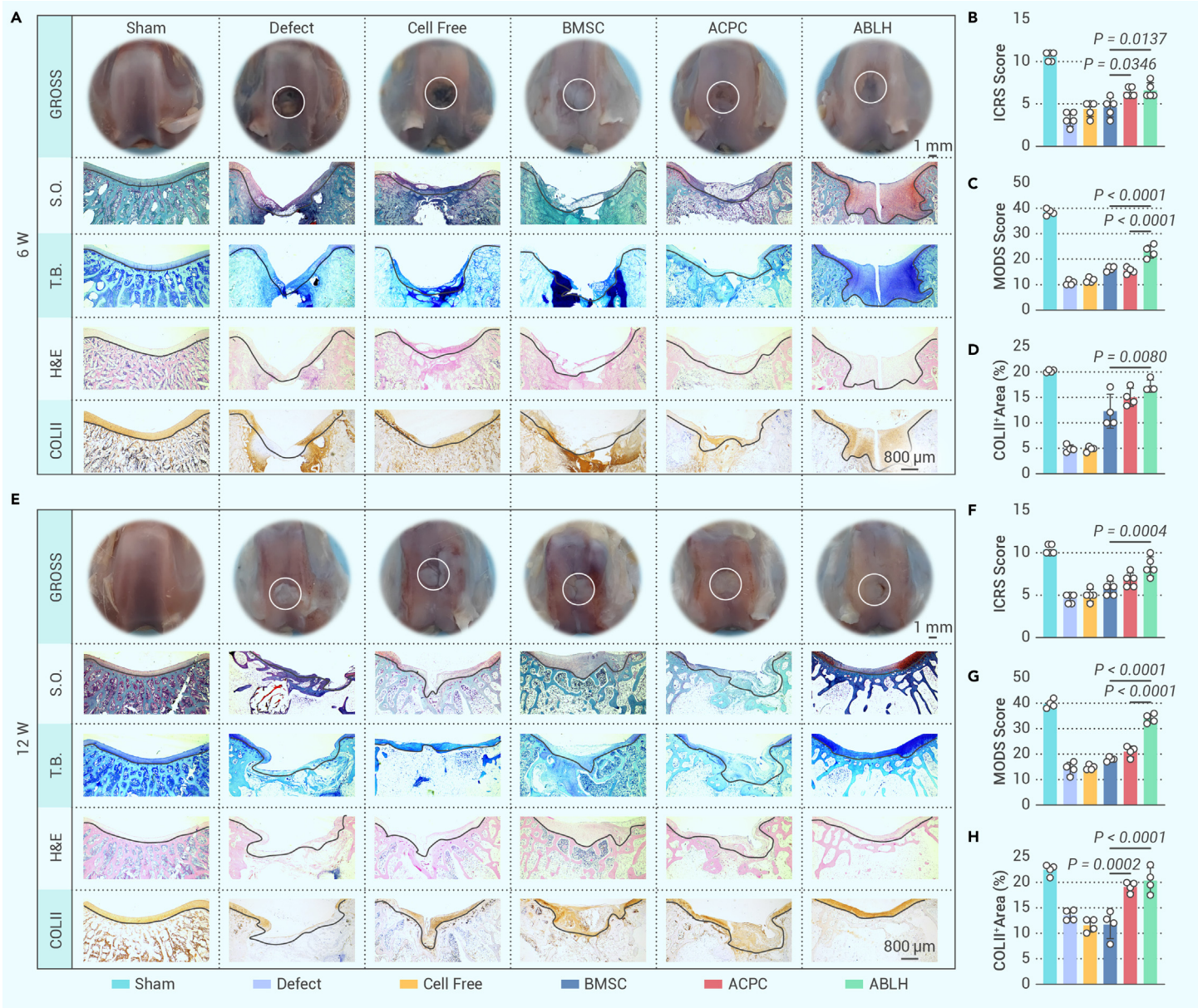

Figure 4. ABLHs promoted cartilage regeneration *in vivo* (A and E) Representative images of gross view, glycosaminoglycan reflected by Safranin O (S.O.), toluidine blue (T.B.), H&E, and cartilage collagen deposition determined by collagen type II IHC staining 6 or 12 weeks postsurgery (black dashed lines indicate the OC interface). (B, C, D, and F) Quantitative analysis International Cartilage Repair Society (ICRS) (n = 5) and Modified O'Driscoll Scale (MODS) assessment (n = 4). (G and H) Quantification of the COLII-positive area in the cartilage phase (n = 4). Data are shown as the mean ± SD. Statistical significance was determined by ANOVA.

natural photosynthetic system, intracellular anabolism can be reprogrammed for the treatment of musculoskeletal diseases.[23] However, the expression levels of bone-specific markers (*Col1a1*, *Alpp*, and *Bglap*) were upregulated in BMSC-laden hydrogels (Figure 3G), coupled with the gradually enhanced O-ECM by alizarin red staining of the mineralized nodules (Figure 3H). The preservation of COLI and osteocalcin (OCN) expression was greatly evident, indicating the optimal conditions provided by bioprinted hydrogels (Figures 3I, 3J, and S8). A pseudotime heatmap supported the dramatically increased expression levels of osteogenic positive–regulated genes GLI family zinc finger 3 (*Gli3*),[24] discoidin domain receptor tyrosine kinase 2 (*Ddr2*),[25] and *Bmp2/4/7*,[26] coinciding with negatively regulated genes midkine (*Mdk*),[27] histone deacetylase 7 (*Hdac7*),[28] and Gremlin 1 (*Grem1*)[29] expression inhibition (Figure 3K). Interestingly, beyond the osteogenesis-related BMP response and ossification pathways, circadian rhythm signaling was identified in BMSC differentiation into the osteoblast lineage (Figures 3L, S8, and S9). Targeting circadian clock–associated hormones such as melatonin has recently emerged as a popular area of research for the maintenance of bone health.[30] The rational allocation of cells in hydrogels exerts an immediate or short-term restorative effect; furthermore, it rebuilds a cell-ECM microenvironment for surrounding cell recruitment and tissue-specific ECM reconstruction in the long-term regenerative process.[31] Taken together, ABLHs achieved ACPC or BMSC commitment toward chondrocytes or osteoblasts in *in vitro* 3D culture, respectively.

ABLHs boosted cartilage phase repair *in vivo*

To explore the potential therapeutic benefits of ABLHs in cartilage or bone regeneration, a full-thickness OC defect model was established in the femoral trochlear groove of rabbits. Samples were collected at 6 or 12 weeks postinjury to evaluate the early and late regenerative capacity of ABLHs. The serum biochemical tests exhibited no anomalies resulting from treatment with hydrogels (Figure S10). Meanwhile, the examination of major organ histopathology revealed no toxic alterations within each group (Figure S11). According to the gross and histomorphometric images at 6 weeks postsurgery, the cartilage phase repair occurred only in the surface consisting mainly of fibrous connective tissue but with scarce collagen- or glycosaminoglycan-rich C-ECM in the defect group. Similarly, cell-free hydrogels showed vulnerable cartilage connections and void bone structures, attributed to the finite supply of endogenous chondrocytes following the degradation of implanted hydrogels (Figures 4A and 4B). In comparison, three cell-laden hydrogels exhibited a relatively intact OC unit benefiting

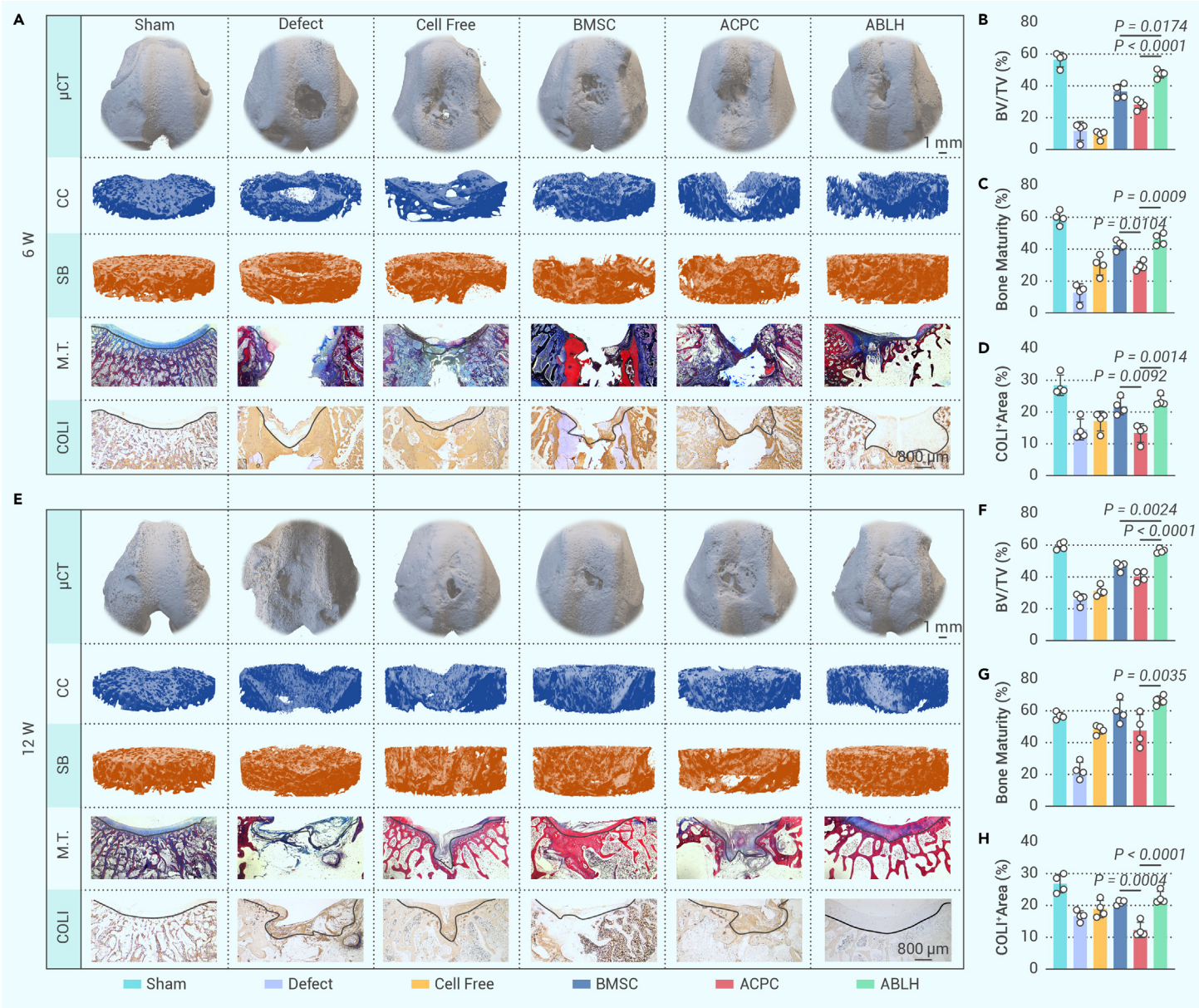

Figure 5. ABLHs accelerated subchondral bone formation and remodeling *in vivo* (A and E) Representative images of bone architecture visualized by 3D reconstructions of the bone surface, calcified cartilage, subchondral bone plate, and bone collagen determined by Masson's trichrome staining (M.T.) or COLI accumulation presented by IHC staining 6 or 12 weeks postsurgery (black dashed lines indicate the OC interface). (B–F) Quantitative analysis of bone volume per tissue volume (BV/TV) (n = 4) and bone maturity assessment (n = 4). (G and H) Quantification of the COLI-positive area in the bone phase (n = 4). Data are shown as the mean ± SD. Statistical significance was determined by ANOVA.

from exogenous stem cell–secreted ECM components. Owing to their robust differentiation potential, BMSC-laden hydrogels formed a cartilaginous matrix-abundant region; more precisely, the newly generated C-ECM was mainly distributed in the subchondral bone. However, comparatively, superior C-ECM deposition at the cartilage layer was demonstrated in the ACPC-laden hydrogels, implying the unignorable importance of spatial regulation in cartilage regeneration, which has universality among different species such as deer[32] or axolotl[33] in nature. More important, ABLHs contributed to the biosynthesis of the most abundant C-ECM located in cartilage and the upper part of the subchondral bone, although the neomatrix was characterized by an irregular arrangement (Figures 4C and 4D). Furthermore, 12 weeks after surgery, except for the incomplete OC unit in the defect group, the morphology reconstruction was finished in the four hydrogel-treated groups. Of these, the degradation products of hydrogels (e.g., gelatin, alginate) act as supplements to C-ECM in cell-free hydrogels and thus help promote cartilage repair.[34] Both BMSC- and ACPC-laden hydrogels reproduced a new OC unit; however, a more complete subchondral bone architecture was shown in the BMSC hydrogels than in the ACPC hydrogels (Figure 4E). Surprisingly, relying on mechanical support by reconstructed stable subchondral bone structure, ABLHs achieved a 23.5% (Figure 4F) higher cartilage regeneration efficacy than ACPC hydrogels (Figures 4G and 4H). Most of the studies on OC integrated repair used prochondrogenic cytokines as accelerators for cartilage regeneration[35]; however, the precise mechanisms by which the TGF-β signaling pathway determines cartilage fate remain elusive. Cao et al. reported that over-activated TGF-β1 in subchondral bone seems to initiate pathological changes in cartilage degeneration.[36] Furthermore, the rapid drug release phenomenon *in vivo* restrains long-term treatment capabilities despite emerging diverse drug delivery systems.[37] Therefore, this study uniquely presents "living hydrogels" based on a pure-bicellular system, cleverly circumventing underlying cytokine-related side effects and high costs. In the initial stage, the implanted living hydrogels remain viable and responsive to surrounding biochemical cues. They undergo a phase of robust proliferation and exhibit remarkable resistance to the immune response. Subsequently, endogenous stem/progenitor cells migrate concomitantly with biomaterial degradation. The regeneration of the OC unit is ultimately achieved through concerted efforts to differentiate chondrocytes or osteoblasts from delivered ACPCs/BMSCs and recruited autologous cells. Using cartilage-derived ACPCs as a convener, articular cartilage reconstruction is driven by exogenous stem cells at an early stage but relayed by amplified cells, initiated endogenous cells, and a suitable environment for tissue development.

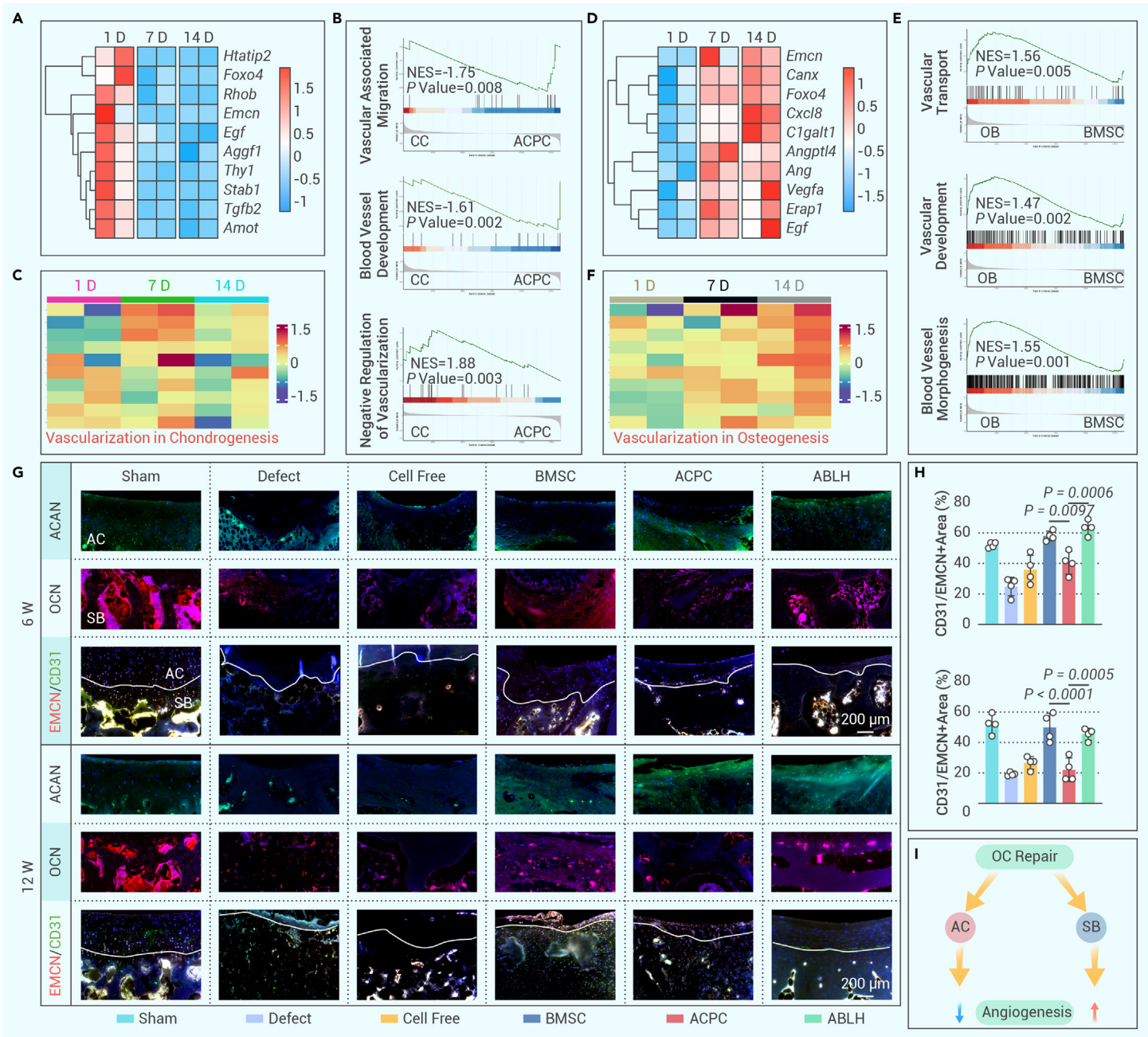

Figure 6. ABLHs coordinated cartilage-bone-vessel crosstalk to reconstruct the OC unit (A and D) Heatmaps of angiogenesis-related DEGs in chondrogenic or osteogenic differentiation. (B and E) GSEA of angiogenesis-related events involved in chondrogenic or osteogenic differentiation. (C and F) GO-based heatmaps of differentially expressed vascularization-associated functions in chondrogenic or osteogenic differentiation. (G) Representative images of ACAN, OCN, and CD31/endomucin double immunofluorescence staining 6 or 12 weeks postsurgery (white dashed lines indicate the OC interface). (H) Quantification of the CD31/endomucin double-positive area in the cartilage and bone phase (n = 4). (I) Schematic illustration of the dichotomous role of angiogenesis in articular cartilage and subchondral bone repair. Data are given as the mean ± SD. Statistical significance was determined by ANOVA.

Collectively, these findings indicate that ABLHs promote the repair and renewal of cartilage.

ABLHs promote bone phase remodeling *in vivo*

The potential therapeutic effects of ABLHs on bone reconstruction were also examined in detail through microcomputed tomography analysis and histological observations. At 6 weeks postimplantation, cell-free hydrogels were of mild but limited utility for bone mass improvement compared with the defect group, indicating that mechanical support alone is not sufficient to drive new bone formation (Figures 5A and 5B). The early structural remodeling in the subchondral bone of the three cell-laden hydrogels was productive, as manifested by abundant blue-stained newly formed bone. However, ACPC hydrogels tended to form a fibrous tissue-like connection at the surface, leaving cystic cavities in the deep layers, which tracks with their inherent commitment toward cartilage (Figures 5C and 5D). Despite advanced bone formation and O-ECM maturation, the fragile and even fractured cartilage layer in BMSC hydrogels severely compromises the regenerative microenvironment,[38] thus impeding chondrocyte survival and C-ECM secretion. ABLHs not only induced bone remodeling in the lower bone layer but also maintained the integrity of the upper cartilage layer, providing suitable cartilage and bone developmental niches. Benefiting from excellent self-repairing capability, at a late stage (12 weeks) after grafting, the reestablishment of the bone defect area was achieved in all of the groups. BMSC-laden hydrogels facilitated trabecular bone regeneration and mature bone formation, based on the large area of red-stained mature bone and brown-stained bone-specific expression of COLI (Figure 5E). By comparison, substantial immature and fibrous-like tissues were observed in ACPC-laden hydrogels, demonstrating that cartilage-derived progenitor cells were of limited capacity for high-quality bone architecture. Remarkably, the bicellular hydrogels implemented biomimetic

bone regeneration with a highly natural microstructure, materialized by 20.8% (Figure 5F) higher bone structural maturity than BMSC-laden hydrogels (Figures 5G and 5H). In contrast to the limited self-regenerative capacity of cartilage, in the OC unit rebuilding process, bone tissue has a substantial capacity for repair and regeneration. Two mechanisms are known for forming bones, referred to as intramembranous or endochondral ossification.[39] Of these, the latter route is mainly involved in OC remodeling. Combining *in vivo* chondrogenic and osteogenic staining, the spatially specific BMSCs in the bicellular hydrogels were subjected to two-stage ossification, indicating the active transition from early cartilage to late bone. Analogously, BMSCs plus microsphere hydrogel-constructed osteo-callus organoids are ready for extremely rapid bone recovery after injury.[40] The individual ACPC hydrogels, however, only produced cartilage-like tissues but failed to provide a potent stimulus for bone tissue. Indeed, the repair of cartilage without bone support at the bottom appears as a castle in the air that leads to the failure of OC repair, and thus continued structural strengthening of bone phase materials has been modified in recent studies.[41] In addition, the influences of ACPCs in the bicellular system on bone remodeling should not be disregarded. As an insulation barrier, the generation of C-ECM can circumvent excessive bone formation to recreate an OC interface.[42] Together, ABLHs accelerate bone generation and maturation.

ABLHs coordinate cartilage-bone-vessel crosstalk for OC unit reconstruction

To further explore the underlying mechanism of powerful renewable ABLH-mediated actions on OC unit reconstruction, the involvement of angiogenesis in C-ECM or O-ECM morphogenesis was intensively studied *in vitro* and *in vivo*. For *in vitro* chondrogenic commitment of ACPC-laden hydrogels, the angiogenesis process gradually diminished over the 2 weeks, reflected in the downregulated expression of angiogenic genes (eg, ras homolog family member B1 [*Rhob*],[43] epidermal growth factor [*Egf*],[44] endomucin [*Emcn*],[45] and vascular endothelial growth factor A [*Vegfa*][46] (Figure 6A). Meanwhile, repressed vessel development was confirmed using gene set enrichment analysis (GSEA) tools (Figure 6B). The heatmap based on Gene Ontology (GO) further showed that early C-ECM morphogenesis was concomitant with new vessel formation, which decreased appreciably following terminal differentiation and maturation (Figure 6C). In contrast, for the osteogenic differentiation of BMSC-laden hydrogels, the expression levels of angiogenin (*Ang*),[47] *Emcn*, *Vegfa*, and *Egf* were gradually upregulated (Figure 6D). GSEA corroborated the progressive formation of blood vessels throughout the differentiation process (Figure 6E). A differential GO term heatmap indicated that angiogenesis, remodeling, and expansion of new blood vessels were indispensable for O-ECM remodeling (Figure 6F). *In vivo* immunofluorescence staining revealed that C-ECM-specific ACAN and O-ECM-specific OCN were distributed spatially in the cartilage or bone layer. Consistent with the above histological staining, BMSC hydrogels tended to promote ossification, whereas those containing ACPCs favored chondrification (Figure 6G). More important, as the specific subtype of the capillary that is associated with osteogenesis, the temporal and spatial expression of type H vessels ($CD31^{hi}$ $Emcn^{hi}$) was evaluated in detail. Type H vessels mainly reside in the subchondral bone region but are rarely detected in articular cartilage[48]; however, the progression of osteoarthritis is accompanied by the increased abundance of type H vessels in subchondral bone and even cartilage invasion.[49] On-target inhibition of type H vessel formation and the relevant TGF-β activity[50] or platelet-derived growth factor subunit-BB signaling[51] benefited cartilage metabolic equilibrium and attenuated osteoarthritis, emphasizing the importance of blood supply deficiency in the cartilage layer.[52] The adverse effects mediated by hypervascularization have been determined recently; nevertheless, finely manipulating stratified vascularization in cartilage or bone layers for OC repair is reported in the present study for the first time. In BMSCs and osteoblast-mediated osteogenic microenvironments, the supply of type H vessels was abundant and even migrated to the upper cartilage layer. Relying on the C-ECM secreted by ACPCs and chondrocytes in bicellular hydrogels, type H vessels were constrained in the bone layer without penetrating and perturbing cartilage homeostasis, which is of great importance to the acquisition of a more harmonious cartilage–bone interface than that seen with homogeneous hydrogels (Figures 6H and S12). In summary, by modulating angiogenesis in distinct phases, ABLHs reconfigured osteoblast-chondrocyte interactions to achieve hierarchical OC unit reconstruction (Figure 6I).

It is important to acknowledge certain limitations that the present study has encountered. First, although our *in vivo* data revealed significant effects of ABLHs on OC regeneration, the precise cell fate regarding proliferation, migration, and differentiation during the repair process remains unvisualized. Due to the identical hydrogels present in both the upper and lower layers, it may prove challenging to establish an absolute distinction between ACPCs and BMSCs in practical terms, particularly following a period of growth and differentiation (Figures 2J and 2K). In fact, the regeneration of the OC unit bears a resemblance to the reproduction of cartilage and bone morphogenesis, wherein effective cellular communication but not isolation is essential for constructing a natural interface between these two tissues.[53] Second, the occurrence of OC defects is frequently accompanied by a synovial inflammatory response, such as aberrant macrophage polarization, which will be thoroughly investigated in our forthcoming research. Third, to more accurately emulate the clinical environment, further advancements should be made in refining the nonhuman primate model.

CONCLUSION

Inspired by the natural hierarchical structure of the OC unit, ABLHs embedded with precursor cells were skillfully built in this study. The 7G3A composite bioink allowed for the direct room temperature printing procedure, maintaining the capacity for cell growth and differentiation. The ability of ACPCs to differentiate into chondrocytes and BMSCs to differentiate into osteoblasts were well preserved in *in vitro* 3D culture systems. More important, *in situ* implantation of ABLHs achieved tissue-specific reconstruction of the upper C-ECM and lower O-ECM layers in an *in vivo* OC defect model. Mechanistically, spatiotemporal regulation of cartilage-bone-vessel crosstalk contributed to ABLH-induced biomimetically OC unit remodeling. Overall, this study proposes a bioadaptive strategy using living cell–based bilayered hydrogels, providing a fundamentally new approach for the efficient repair of OC defects.

MATERIALS AND METHODS

See supplemental information for details.

REFERENCES

1. Lesage, C., Lafont, M., Guihard, P., Weiss, P., Guicheux, J., and Delplace, V. (2022). Material-Assisted Strategies for Osteochondral Defect Repair. Adv. Sci. ***9***, e2200050.
2. Li, W., Lai, J., Zu, Y., et al. (2022). Cartilage-inspired hydrogel lubrication strategy. Innovation ***3***, 100275.
3. Hu, X., Wang, Y., Tan, Y., Wang, J., Liu, H., Wang, Y., Yang, S., Shi, M., Zhao, S., Zhang, Y., and Yuan, Q. (2017). A Difunctional Regeneration Scaffold for Knee Repair based on Aptamer-Directed Cell Recruitment. Adv. Mater. ***29***, 1605235.
4. Ma, Z., Song, W., He, D., Zhang, X., He, Y., and Li, H. (2022). Smart μ-Fiber Hydrogels with Macro-Porous Structure for Sequentially Promoting Multiple Phases of Articular Cartilage Regeneration. Adv. Funct. Mater. ***32***, 2113380.
5. Gao, F., Xu, Z., Liang, Q., Liu, B., Li, H., Wu, Y., Zhang, Y., Lin, Z., Wu, M., Ruan, C., and Liu, W. (2018). Direct 3D Printing of High Strength Biohybrid Gradient Hydrogel Scaffolds for Efficient Repair of Osteochondral Defect. Adv. Funct. Mater. ***28***, 1706644.
6. Sun, Y., You, Y., Jiang, W., Wang, B., Wu, Q., and Dai, K. (2020). 3D bioprinting dual-factor releasing and gradient-structured constructs ready to implant for anisotropic cartilage regeneration. Sci. Adv. ***6***, eaay1422.
7. Kang, Y., Zhang, H., Chen, L., Dong, J., Yao, B., Yuan, X., Qin, D., Yaremenko, A.V., Liu, C., Feng, C., Ji, X., and Tao, W. (2022). The marriage of Xenes and hydrogels: Fundamentals, applications, and outlook. Innovation ***3***, 100327.
8. Qiao, Z., Lian, M., Han, Y., Sun, B., Zhang, X., Jiang, W., Li, H., Hao, Y., and Dai, K. (2021). Bioinspired stratified electrowritten fiber-reinforced hydrogel constructs with layer-specific induction capacity for functional osteochondral regeneration. Biomaterials ***266***, 120385.
9. Liu, Y., Peng, L., Li, L., Huang, C., Shi, K., Meng, X., Wang, P., Wu, M., Li, L., Cao, H., Wu, K., Zeng, Q., Pan, H., Lu, W.W., Qin, L., Ruan, C., and Wang, X. (2021). 3D-bioprinted BMSC-laden biomimetic multiphasic scaffolds for efficient repair of osteochondral defects in an osteoarthritic rat model. Biomaterials ***279***, 121216.
10. Shaw, S., and White, J.D. (2019). Asymmetric Catalysis Using Chiral Salen-Metal Complexes: Recent Advances. Chem. Rev. ***119***, 9381–9426.
11. He, H., Li, D., Lin, Z., Peng, L., Yang, J., Wu, M., Cheng, D., Pan, H., and Ruan, C. (2020). Temperature-programmable and enzymatically solidifiable gelatin-based bioinks enable facile extrusion bioprinting. Biofabrication ***12***, 045003.
12. Keller, L., Pijnenburg, L., Idoux-Gillet, Y., Bornert, F., Benameur, L., Tabrizian, M., Auvray, P., Rosset, P., María Gonzalo-Daganzo, R., Gómez Barrena, E., Gentile, L., and Benkirane-Jessel, N. (2019). Preclinical safety study of a combined therapeutic bone wound dressing for osteoarticular regeneration. Nat. Commun. ***10***, 2156.
13. Liu, X., Chen, Y., Mao, A.S., Xuan, C., Wang, Z., Gao, H., An, G., Zhu, Y., Shi, X., and Mao, C. (2020). Molecular recognition-directed site-specific release of stem cell differentiation inducers for enhanced joint repair. Biomaterials ***232***, 119644.

14. Blaeser, A., Duarte Campos, D.F., Puster, U., Richtering, W., Stevens, M.M., and Fischer, H. (2016). Controlling Shear Stress in 3D Bioprinting is a Key Factor to Balance Printing Resolution and Stem Cell Integrity. Adv. Healthc. Mater. **5**, 326–333.
15. Hallett, S.A., Matsushita, Y., Ono, W., Sakagami, N., Mizuhashi, K., Tokavanich, N., Nagata, M., Zhou, A., Hirai, T., Kronenberg, H.M., and Ono, N. (2021). Chondrocytes in the resting zone of the growth plate are maintained in a Wnt-inhibitory environment. Elife **10**, e64513.
16. Liu, H., Lan, Y., Xu, J., Chang, C.F., Brugmann, S.A., and Jiang, R. (2013). Odd-skipped related-1 controls neural crest chondrogenesis during tongue development. Proc. Natl. Acad. Sci. USA **110**, 18555–18560.
17. Otsuki, S., Hanson, S.R., Miyaki, S., Grogan, S.P., Kinoshita, M., Asahara, H., Wong, C.H., and Lotz, M.K. (2010). Extracellular sulfatases support cartilage homeostasis by regulating BMP and FGF signaling pathways. Proc. Natl. Acad. Sci. USA **107**, 10202–10207.
18. Tsumaki, N., Nakase, T., Miyaji, T., Kakiuchi, M., Kimura, T., Ochi, T., and Yoshikawa, H. (2002). Bone morphogenetic protein signals are required for cartilage formation and differently regulate joint development during skeletogenesis. J. Bone Miner. Res. **17**, 898–906.
19. van den Bosch, M.H., Blom, A.B., Kram, V., Maeda, A., Sikka, S., Gabet, Y., Kilts, T.M., van den Berg, W.B., van Lent, P.L., van der Kraan, P.M., and Young, M.F. (2017). WISP1/CCN4 aggravates cartilage degeneration in experimental osteoarthritis. Osteoarthritis Cartilage **25**, 1900–1911.
20. Tillgren, V., Ho, J.C.S., Önnerfjord, P., et al. (2015). The novel small leucine-rich protein chondroadherin-like (CHADL) is expressed in cartilage and modulates chondrocyte differentiation. J. Biol. Chem. **290**, 918–925.
21. Zhu, S., Donovan, E.L., Makosa, D., Mehta-D'souza, P., Jopkiewicz, A., Batushansky, A., Cortassa, D., Simmons, A.D., Lopes, E.B.P., Kinter, M., and Griffin, T.M. (2022). Sirt3 Promotes Chondrogenesis, Chondrocyte Mitochondrial Respiration and the Development of High-Fat Diet-Induced Osteoarthritis in Mice. J. Bone Miner. Res. **37**, 2531–2547.
22. Zhang, Y., Liu, Y., Hou, M., Xia, X., Liu, J., Xu, Y., Shi, Q., Zhang, Z., Wang, L., Shen, Y., Yang, H., He, F., and Zhu, X. (2023). Reprogramming of Mitochondrial Respiratory Chain Complex by Targeting SIRT3-COX4I2 Axis Attenuates Osteoarthritis Progression. Adv. Sci. **10**, e2206144.
23. Chen, P., Liu, X., Gu, C., Zhong, P., Song, N., Li, M., Dai, Z., Fang, X., Liu, Z., Zhang, J., Tang, R., Fan, S., and Lin, X. (2022). A plant-derived natural photosynthetic system for improving cell anabolism. Nature **612**, 546–554.
24. Litingtung, Y., Dahn, R.D., Li, Y., Fallon, J.F., and Chiang, C. (2002). Shh and Gli3 are dispensable for limb skeleton formation but regulate digit number and identity. Nature **418**, 979–983.
25. Mohamed, F.F., Ge, C., Cowling, R.T., Lucas, D., Hallett, S.A., Ono, N., Binrayes, A.A., Greenberg, B., and Franceschi, R.T. (2022). The collagen receptor, discoidin domain receptor 2, functions in Gli1-positive skeletal progenitors and chondrocytes to control bone development. Bone Res. **10**, 11.
26. Salazar, V.S., Gamer, L.W., and Rosen, V. (2016). BMP signalling in skeletal development, disease and repair. Nat. Rev. Endocrinol. **12**, 203–221.
27. Neunaber, C., Catala-Lehnen, P., Beil, F.T., Marshall, R.P., Kanbach, V., Baranowsky, A., Lehmann, W., Streichert, T., Ignatius, A., Muramatsu, T., Schinke, T., and Amling, M. (2010). Increased trabecular bone formation in mice lacking the growth factor midkine. J. Bone Miner. Res. **25**, 1724–1735.
28. Jensen, E.D., Schroeder, T.M., Bailey, J., Gopalakrishnan, R., and Westendorf, J.J. (2008). Histone deacetylase 7 associates with Runx2 and represses its activity during osteoblast maturation in a deacetylation-independent manner. J. Bone Miner. Res. **23**, 361–372.
29. Nolan, K., Kattamuri, C., Rankin, S.A., Read, R.J., Zorn, A.M., and Thompson, T.B. (2016). Structure of Gremlin-2 in Complex with GDF5 Gives Insight into DAN-Family-Mediated BMP Antagonism. Cell Rep. **16**, 2077–2086.
30. Munmun, F., and Witt-Enderby, P.A. (2021). Melatonin effects on bone: Implications for use as a therapy for managing bone loss. J. Pineal Res. **71**, e12749.
31. Chen, W., Chen, H., Zheng, D., Zhang, H., Deng, L., Cui, W., Zhang, Y., Santos, H.A., and Shen, H. (2020). Gene-Hydrogel Microenvironment Regulates Extracellular Matrix Metabolism Balance in Nucleus Pulposus. Adv. Sci. **7**, 1902099.
32. Qin, T., Zhang, G., Zheng, Y., Li, S., Yuan, Y., Li, Q., Hu, M., Si, H., Wei, G., Gao, X., Cui, X., Xia, B., Ren, J., Wang, K., Ba, H., Liu, Z., Heller, R., Li, Z., Wang, W., Huang, J., Li, C., and Qiu, Q. (2023). A population of stem cells with strong regenerative potential discovered in deer antlers. Science **379**, 840–847.
33. Qin, T., Fan, C.M., Wang, T.Z., Sun, H., Zhao, Y.Y., Yan, R.J., Yang, L., Shen, W.L., Lin, J.X., Bunpetch, V., Cucchiarini, M., Clement, N.D., Mason, C.E., Nakamura, N., Bhonde, R., Yin, Z., and Chen, X. (2021). Single-cell RNA-seq reveals novel mitochondria-related musculoskeletal cell populations during adult axolotl limb regeneration process. Cell Death Differ. **28**, 1110–1125.
34. Klotz, B.J., Gawlitta, D., Rosenberg, A.J.W.P., Malda, J., and Melchels, F.P.W. (2016). Gelatin-Methacryloyl Hydrogels: Towards Biofabrication-Based Tissue Repair. Trends Biotechno **34**, 394–407.
35. Jiang, Y., and Tuan, R.S. (2015). Origin and function of cartilage stem/progenitor cells in osteoarthritis. Nat. Rev. Rheumatol. **11**, 206–212.
36. Zhen, G., Wen, C., Jia, X., Li, Y., Crane, J.L., Mears, S.C., Askin, F.B., Frassica, F.J., Chang, W., Yao, J., Carrino, J.A., Cosgarea, A., Artemov, D., Chen, Q., Zhao, Z., Zhou, X., Riley, L., Sponseller, P., Wan, M., Lu, W.W., and Cao, X. (2013). Inhibition of TGF-β signaling in mesenchymal stem cells of subchondral bone attenuates osteoarthritis. Nat. Med. **19**, 704–712.
37. Lam, J., Lu, S., Kasper, F.K., et al. (2015). Strategies for controlled delivery of biologics for cartilage repair. Adv. Drug Deliv. Rev. **84**, 123–134.
38. Yang, R., Li, G., Zhuang, C., Yu, P., Ye, T., Zhang, Y., Shang, P., Huang, J., Cai, M., Wang, L., Cui, W., and Deng, L. (2021). Gradient bimetallic ion-based hydrogels for tissue microstructure reconstruction of tendon-to-bone insertion. Sci. Adv. **7**, eabg3816.
39. Xie, L., Wang, G., Wu, Y., Liao, Q., Mo, S., Ren, X., Tong, L., Zhang, W., Guan, M., Pan, H., Chu, P.K., and Wang, H. (2021). Programmed surface on poly(aryl-ether-ether-ketone) initiating immune mediation and fulfilling bone regeneration sequentially. Innovation **2**, 100148.
40. Xie, C., Liang, R., Ye, J., Peng, Z., Sun, H., Zhu, Q., Shen, X., Hong, Y., Wu, H., Sun, W., Yao, X., Li, J., Zhang, S., Zhang, X., and Ouyang, H. (2022). High-efficient engineering of osteo-callus organoids for rapid bone regeneration within one month. Biomaterials **288**, 121741.
41. Levingstone, T.J., Ramesh, A., Brady, R.T., Brama, P.A.J., Kearney, C., Gleeson, J.P., and O'Brien, F.J. (2016). Cell-free multi-layered collagen-based scaffolds demonstrate layer specific regeneration of functional osteochondral tissue in caprine joints. Biomaterials **87**, 69–81.
42. Wang, X., Lin, J., Li, Z., Ma, Y., Zhang, X., He, Q., Wu, Q., Yan, Y., Wei, W., Yao, X., Li, C., Li, W., Xie, S., Hu, Y., Zhang, S., Hong, Y., Li, X., Chen, W., Duan, W., and Ouyang, H. (2022). Identification of an Ultrathin Osteochondral Interface Tissue with Specific Nanostructure at the Human Knee Joint. Nano Lett. **22**, 2309–2319.
43. Gerald, D., Adini, I., Shechter, S., Perruzzi, C., Varnau, J., Hopkins, B., Kazerounian, S., Kurschat, P., Blachon, S., Khedkar, S., Bagchi, M., Sherris, D., Prendergast, G.C., Klagsbrun, M., Stuhlmann, H., Rigby, A.C., Nagy, J.A., and Benjamin, L.E. (2013). RhoB controls coordination of adult angiogenesis and lymphangiogenesis following injury by regulating VEZF1-mediated transcription. Nat Commu **4**, 2824.
44. Bentz, G.L., and Yurochko, A.D. (2008). Human CMV infection of endothelial cells induces an angiogenic response through viral binding to EGF receptor and beta1 and beta3 integrins. Proc. Natl. Acad. Sci. USA **105**, 5531–5536.
45. Xu, R., Yallowitz, A., Qin, A., Wu, Z., Shin, D.Y., Kim, J.M., Debnath, S., Ji, G., Bostrom, M.P., Yang, X., Zhang, C., Dong, H., Kermani, P., Lalani, S., Li, N., Liu, Y., Poulos, M.G., Wach, A., Zhang, Y., Inoue, K., Di Lorenzo, A., Zhao, B., Butler, J.M., Shim, J.H., Glimcher, L.H., and Greenblatt, M.B. (2018). Targeting skeletal endothelium to ameliorate bone loss. Nat. Med. **24**, 823–833.
46. Usui-Ouchi, A., and Friedlander, M. (2019). Anti-VEGF therapy: higher potency and long-lasting antagonism are not necessarily better. J. Clin. Invest. **129**, 3032–3034.
47. Liu, X., Chai, Y., Liu, G., Su, W., Guo, Q., Lv, X., Gao, P., Yu, B., Ferbeyre, G., Cao, X., and Wan, M. (2021). Osteoclasts protect bone blood vessels against senescence through the angiogenin/plexin-B2 axis. Nat. Commun. **12**, 1832.
48. Hu, W., Chen, Y., Dou, C., et al. (2021). Microenvironment in subchondral bone: predominant regulator for the treatment of osteoarthritis. Ann. Rheum. Dis. **80**, 413–422.
49. Lu, J., Zhang, H., Cai, D., Zeng, C., Lai, P., Shao, Y., Fang, H., Li, D., Ouyang, J., Zhao, C., Xie, D., Huang, B., Yang, J., Jiang, Y., and Bai, X. (2018). Positive-Feedback Regulation of Subchondral H-Type Vessel Formation by Chondrocyte Promotes Osteoarthritis Development in Mice. J. Bone Miner. Res. **33**, 909–920.
50. Cui, Z., Crane, J., Xie, H., Jin, X., Zhen, G., Li, C., Xie, L., Wang, L., Bian, Q., Qiu, T., Wan, M., Xie, M., Ding, S., Yu, B., and Cao, X. (2016). Halofuginone attenuates osteoarthritis by inhibition of TGF-β activity and H-type vessel formation in subchondral bone. Ann. Rheum. Dis. **75**, 1714–1721.
51. Cui, Z., Wu, H., Xiao, Y., Xu, T., Jia, J., Lin, H., Lin, R., Chen, K., Lin, Y., Li, K., Wu, X., Li, C., and Yu, B. (2022). Endothelial PDGF-BB/PDGFR-β signaling promotes osteoarthritis by enhancing angiogenesis-dependent abnormal subchondral bone formation. Bone Res. **10**, 58.
52. Wang, X., Wu, Q., Zhang, R., Fan, Z., Li, W., Mao, R., Du, Z., Yao, X., Ma, Y., Yan, Y., Sun, W., Wu, H., Wei, W., Hu, Y., Hong, Y., Hu, H., Koh, Y.W., Duan, W., Chen, X., and Ouyang, H. (2023). Stage-specific and location-specific cartilage calcification in osteoarthritis development. Ann. Rheum. Dis. **82**, 393–402.
53. Aghajanian, P., and Mohan, S. (2018). The art of building bone: emerging role of chondrocyte-to-osteoblast transdifferentiation in endochondral ossification. Bone Res. **6**, 19.

ACKNOWLEDGMENTS

This work was supported by grants from the National Key R&D Program of China (Grant Nos. 2018YFA0703100 and 2022YFC2502902), the National Nature Science Foundation of China (Grant Nos. 82072442, 82272494, 82072082, 32122046, 32101102), the Orthopaedic Medical Innovation Center of Jiangsu (CXZX202209), Key Laboratory of Orthopaedics of Suzhou (SZS2022017), the Priority Academic Program Development of Jiangsu Higher Education Institutions (PAPD), and the Shenzhen Fundamental Research Foundation (Grant Nos. JSGG20210629144537007, JCYJ20210324115814040, and JCYJ20210324113001005).

AUTHOR CONTRIBUTIONS

Y.Z., H.Y., X.Z., and C.R. conceived the idea and designed the experiments. Y.Z., D. Li, Y.L., L.P., D. Lu, and P.W. performed the experiments. Y.Z., D. Li, and Y.L. analyzed the data with the assistance of D.K. Y.Z., D. Li, and C.R. wrote the manuscript. C.R. and X.Z. supervised the project.

DECLARATION OF INTERESTS

The authors declare no competing interests.

SUPPLEMENTAL INFORMATION

It can be found online at https://doi.org/10.1016/j.xinn.2023.100542.

LEAD CONTACT WEBSITE

http://htod.siat.ac.cn/index.php/Team/detail.shtml?id=8&cid=11.